Research Article

Rectifying effect in a MoS_2 monolayer crossed with an electro-spun PEDOT-PSS nano-ribbon

Kelotchi S. Figueroa[1] · Jose L. Pérez[1] · Ahmad Matar[1] · Idalia Ramos[1] · Nicholas J. Pinto[1] · Meng-Qiang Zhao[2] · A. T. Charlie Johnson[2]

Abstract

A chemical vapor-deposited monolayer MoS_2 crystal was crossed with an electro-spun PEDOT-PSS nano-ribbon under ambient conditions. The current–voltage (*I–V*) curve measured across the hetero-junction was nonlinear and asymmetric, similar to a diode. Under thermal equilibrium, electrons flowed from the MoS_2 conduction band into the PEDOT-PSS LUMO level. This occurred via band bending that established a constant Fermi level across the interface. Consequently, a potential barrier was formed that restricted the current. Under normal operation in air, the diode turn-on voltage was 0.1 V and the rectification ratio at ± 1 V was 20. The thermionic emission Schottky junction model was employed for data analysis. The ideality factor was 1.9, and height of the barrier was 0.18 eV. The easy fabrication, low turn-on voltage and high rectification ratio could make this diode useful in cheap, low-power-consumption signal rectifiers.

Keywords MoS_2 · PEDOT-PSS · Nano-ribbon · Diode

1 Introduction

The layered transition metal dichalcogenide (TMD) MoS_2 belongs to a family of two-dimensional electronic materials similar to graphene [1]. In its monolayer form, a hexagonally arranged planar sheet of Mo atoms is sandwiched between two planar sheets of S atoms [2]. The thickness of a single S–Mo–S layer is ~ 0.7 nm [3], and van der Waals attractive forces between layers result in the formation of bulk MoS_2 crystals. Manual exfoliation of macroscopic crystals [4–7] and chemical vapor deposition (CVD) [8–12] are some of the techniques used to obtain MoS_2 monolayers. Like graphene, MoS_2 is stable in air; however, unlike graphene MoS_2 has a finite bandgap that varies from 1.2 eV (indirect) in the bulk [13] to 1.8 eV (direct) in a monolayer [1]. MoS_2 therefore exhibits useful semiconducting properties. The electronic configuration of *d* subshell electrons in Mo together with S vacancies result in MoS_2 being an *n*-type semiconductor [2]. Stable *n*-type materials are uncommon and hence desirable, especially in fabricating complementary electronic devices. Of the various TMDs currently known, MoS_2 is one of the most widely studied materials. While TMDs are popular industrial dry film lubricants, fabricating electronic devices from these materials extends their utility beyond tribological applications.

Diodes play an important role in converting AC to DC in power supplies and other electronic applications. A Schottky diode can be fabricated by forming a junction of an *n*-type semiconductor and a *p*-doped conducting polymer [14]. The effective turn-on voltages in Schottky diodes are lower than that of *p–n* junction diodes. Also, being a majority carrier device, Schottky diodes lack diffusion capacitance and hence can operate at higher frequencies [15]. Recently, we fabricated and analyzed a Schottky diode by crossing monolayer *n*-WS_2 with a poly(3,4-ethylenedioxythiophene) doped with poly(styrene sulfonic acid)—PEDOT-PSS nano-ribbon [16]. This paper extends the previous work to include a similar device, where

✉ Nicholas J. Pinto, nicholas.pinto@upr.edu | [1]Department of Physics and Electronics, University of Puerto Rico-Humacao, Humacao, PR 00791, USA. [2]Department of Physics and Astronomy, University of Pennsylvania, Philadelphia, PA 19104, USA.

SN Applied Sciences (2019) 1:574 | https://doi.org/10.1007/s42452-019-0595-0

Received: 27 February 2019 / Accepted: 10 May 2019 / Published online: 16 May 2019

monolayer MoS_2 is crossed with a PEDOT-PSS nano-ribbon. On comparing the WS_2/PEDOT-PSS and MoS_2/PEDOT-PSS diodes, the ideality parameters were similar for both diodes (1.9). However, the MoS_2/PEDOT-PSS diode had a lower turn-on voltage (0.1 V compared to 1.4 V). In addition, it possessed a higher rectification ratio (20 compared to 12) and a smaller barrier height (0.18 eV compared to 0.58 eV). The MoS_2/PEDOT-PSS diode was therefore superior to the WS_2/PEDOT-PSS diode, with greater potential for practical applications. The Ag contacts (with a lower Fermi energy) used in the MoS_2/PEDOT-PSS diode (compared to Au contacts used to for other) lower the contact resistance. Combining this with the smaller bandgap in MoS_2 (1.8 eV) compared to WS_2 (2.0 eV) would lead to better charge injection into MoS_2 due to the reduced barrier height. Finally, WS_2 is partially soluble in water, while MoS_2 is insoluble [17], and this would affect the surface states in WS_2 increasing the barrier height [18] for the WS_2/PEDOT-PSS diode.

2 Experimental

Controlled growth of monolayer MoS_2 on Si^+/SiO_2 substrates used in this work has been reported elsewhere [19]. After growth, the MoS_2 crystals were transferred to clean pre-patterned or un-patterned Si^+/SiO_2 substrates (200 nm oxide thickness) via the use of a spin-coated PMMA film and a subsequent KOH oxide etch [20]. Some reasons for this transfer were: to avoid the possibility of using a substrate with a damaged oxide layer during CVD growth; to use new substrates that were pre-patterned and hence useful in a field-effect transistor configuration (FET); to increase the spacing between MoS_2 crystals on the new substrates, and hence fabricate an isolated MoS_2/PEDOT-PSS junction that eliminates cross-interference from other diodes. The adhesion of MoS_2 to the fresh substrates was sufficiently strong since solvent washing did not lead to delamination. Figure 1a shows a transmission electron microscope (TEM) image of isolated MoS_2 crystals, with a characteristic equilateral triangular shape. Figure 1b shows a representative Raman spectrum of the MoS_2 crystals used in this study. The peak at 383 cm^{-1} corresponds to the in-plane E^1_{2g} mode, while the peak at 404 cm^{-1} corresponds to the out-of-plane A_{1g} mode [21]. Figure 1c shows an atomic force microscope (AFM) image of an isolated as-grown single MoS_2 crystal together with a height profile along the black scan line seen in Fig. 1d. The height of the crystal from the AFM measurement is ~ 0.9 nm, which together with the Raman peak separation of 21 cm^{-1} confirm that the MoS_2 crystals are one layer thick [21, 22].

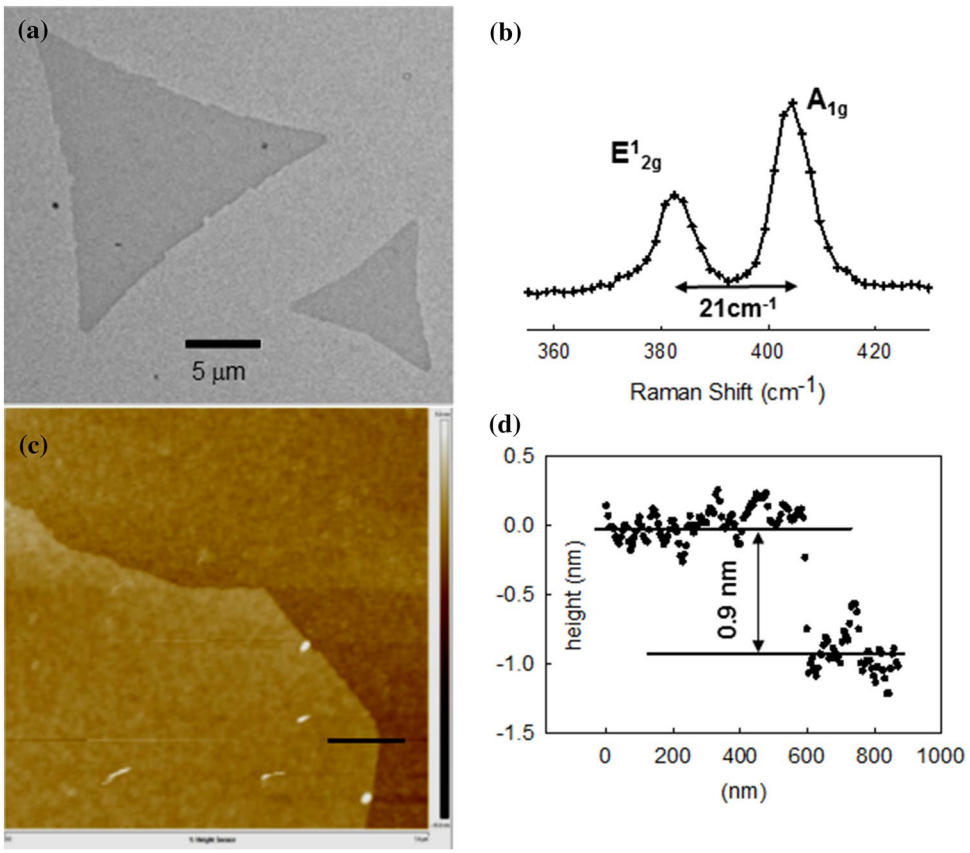

Fig. 1 **a** TEM image of isolated CVD-grown MoS_2 crystals. **b** Raman spectrum of MoS_2 showing two peaks characteristic of MoS_2 single crystals. **c** AFM image of a section of a MoS_2 crystal. **d** Height profile along the black line shown in **c**

Commercial PEDOT-PSS was obtained from Agfa Gevaert N.V. as an aqueous dispersion. A 2 wt% of polyethylene oxide (PEO) was dissolved in it and used to fabricate ribbons. Using the electrospinning technique, nano-ribbons having widths of a few micrometers and height ~ 10 nm were prepared in air [23]. By quickly intercepting the electro-spun jet with the substrate containing MoS_2 crystals, isolated PEDOT-PSS nano-ribbons land on it at random. All these nano-ribbons stick to the substrate, and some also cross over the MoS_2 crystals as shown in Fig. 2a. Using a suitable TEM grid as a shadow mask, Ag contact electrodes were then evaporated after the grid was positioned in such a way that the grid bars covered the junction formed at the intersection of the MoS_2 and PEDOT-PSS. The advantage of using a TEM grid as a shadow mask for contact electrodes is that this strategy eliminates the need for harsh chemicals typically used in optical lithography and lift-off procedures. This technique preserves the conducting polymer component of the device from decomposition, and the device shape parameters were easily determined with a 100 × compound microscope. The silver contact pads are shown in Fig. 2b after evaporation, with the grid removed. Figure 2c shows a schematic image of the external electrical connections to the device.

The device was electrically characterized in air using a Keithley electrometer model 6517A. For the three terminal field-effect transistor characterizations, an additional Keithley 2400 source meter supplied the gate bias. All the measurements were made at room temperature.

3 Results and discussion

Prior to investigating the diode, PEDOT-PSS and MoS_2 were electrically characterized separately. A PEDOT-PSS nano-ribbon was captured on un-patterned Si^+/SiO_2 substrates and a TEM grid used to place contact pads on the ribbon as explained earlier. Figure 3 shows the current–voltage (I_{DS}–V_{DS}) curve for this nano-ribbon when used in a FET configuration. The inset to Fig. 3 shows an image of the nano-ribbon lying between two electrodes—the source (S) and drain (D). The ribbon (channel) length between the two contacts was 55 µm, and its thickness was 10 nm. The I_{DS}–V_{DS} curves in Fig. 3 corresponding to this device are symmetric and Ohmic, suggesting the absence of any Schottky barriers with the electrodes. In addition, there is no change in the channel resistance for different back-gate (G) voltages up to ± 30 V. The absence of a field effect could

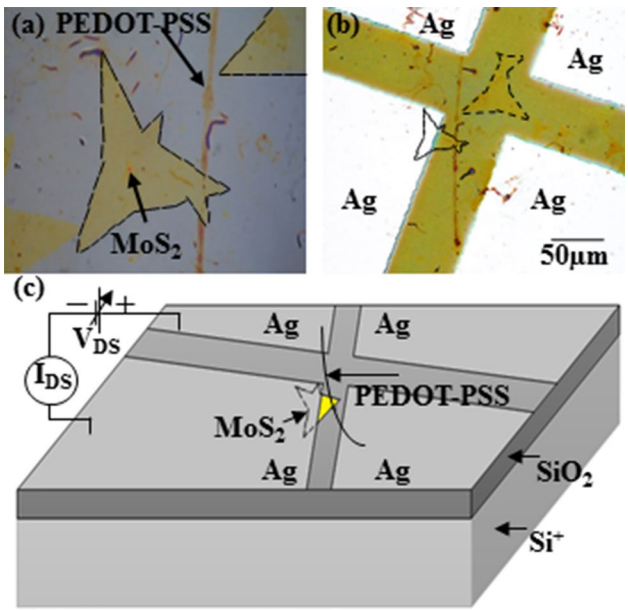

Fig. 2 **a** Microscope image of an electro-spun PEDOT-PSS nano-ribbon crossing a MoS_2 monolayer crystal. **b** A lower magnification image of **a** after using a TEM grid as a shadow mask and evaporating Ag electrodes. The grid bars covered the PEDOT-PSS/MoS_2 intersection during evaporation. The dashed lines represent the edges of the MoS_2 crystals. Four Ag contacts can be seen, two of which contact the PEDOT-PSS nano-ribbon and one contacting the MoS_2 crystal. The fourth contact is open. **c** Simplified schematic diagram of the device shown in **b** together with the external electrical circuit

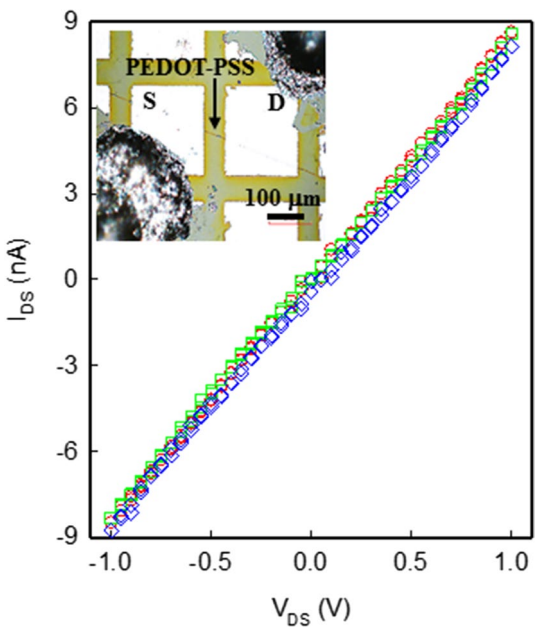

Fig. 3 Drain–source current (I_{DS}) versus drain–source voltage (V_{DS}) curves measured in vacuum of the PEDOT-PSS nano-ribbon for different back-gate voltages; red 0 V—(open circle); green − 30 V—(open square); blue + 30 V—(open diamond). Inset: PEDOT-PSS nano-ribbon lying between two Ag contact electrodes (S/D). Ag epoxy (seen at opposite corners) was used to hard-wire the device

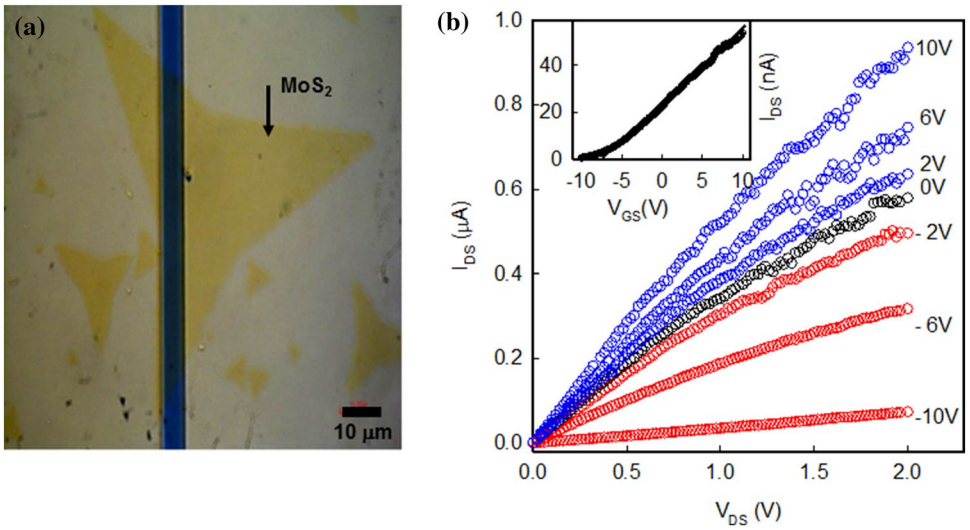

Fig. 4 **a** Optical microscope image of a MoS_2 crystal bridging two electrodes. **b** Drain–source current (I_{DS}) versus drain–source voltage (V_{DS}) curves measured in vacuum for various back-gate bias voltages (V_{GS}). The gate bias V_{GS} is shown to the right above each curve. Inset: drain–source current (I_{DS}) versus gate–source voltage (V_{GS}) for fixed $V_{DS} = 0.1$ V

be due to screening of the electric field by highly conducting islands within the polymer [24] combined with the low dielectric permittivity of the gate insulator (SiO_2). The Fermi level in PEDOT-PSS (E_{FP}) is assumed to stay pinned midway between the LUMO and HUMO levels. The nano-ribbon conductivity was 0.23 S/cm, lower than reported earlier [16] due to a slightly larger fraction of PEO in the present composite nano-ribbon. The lower conductivity, however, does not affect diode operation.

Figure 4a shows an image of a MoS_2 monolayer transferred to a pre-patterned Si^+/SiO_2 substrate. The MoS_2 sample is seen bridging two electrodes (S/D) 4 μm apart. Figure 4b shows the I_{DS}–V_{DS} curves of the device when connected in a FET configuration. For each back-gate voltage, the current tends to saturate for $V_{DS} > 0.5$ V after an initial linear increase. Such measurements were made on numerous devices. All devices showed an increase in I_{DS} for increasing V_{GS}. This implies that MoS_2 is an *n*-type semiconductor [2]. Without a gate voltage, there is no induced charge in the channel and the conductivity was calculated to be 1.1 S/cm. This value is consistent with un-doped semiconductors (amorphous Si). The inset to Fig. 4b shows the device trans-conductance (I_{DS}–V_{GS}) curve that is consistent with the I_{DS}–V_{DS} measurements. From the linear portion of this curve, the trans-conductance was calculated to be 3.3 nS and the mobility was 0.5 cm^2/V s.

Figure 5 shows the *I*–*V* characteristics of the MoS_2/PEDOT-PSS diode shown in Fig. 2b. The electrode contacting PEDOT-PSS was first connected to the source voltage positive terminal and the negative terminal to the MoS_2 arm. There is a linear current increase for increasing voltage as seen in the figure. The device is then turned on in the first quadrant for $V > 0.1$ V. This is the forward bias condition of a diode [14]. The current was negligible under reverse bias. Reversing the voltage supply connections and repeating the experiment enable diode turn on in the third quadrant as seen in Fig. 5. The nonlinear asymmetric curve is primarily due to the Schottky junction formed where PEDOT-PSS crosses MoS_2, and is not due to the metal/MoS_2 or metal/PEDOT-PSS contacts. Comparable values of the conductivity in PEDOT-PSS and mobility in MoS_2 suggest that the contact resistance is insignificant and does not affect diode performance. The on/off ratio calculated by dividing the on current at + 1 V to the off current at − 1 V was 20. This value depends on the off state current, the device series resistance and the barrier

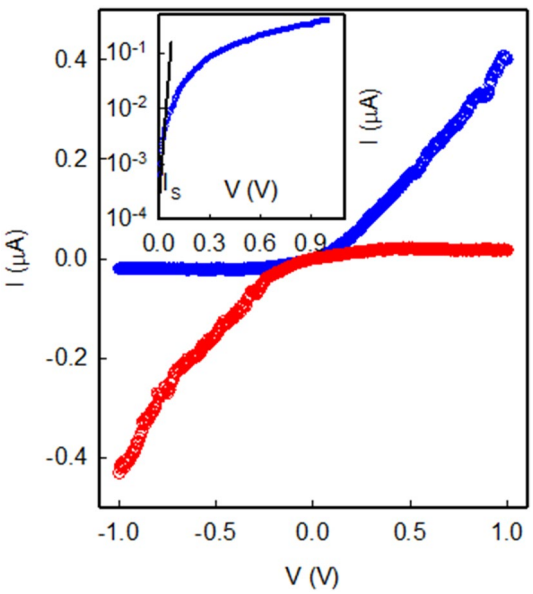

Fig. 5 *I*–*V* curve measured in air for the device seen in Fig. 2b with the voltage source positive terminal connected to PEDOT-PSS and the negative to MoS_2 (blue). The red curve is the same *I*–*V* with the external connections reversed. Inset: semi-logarithmic plot of the current as a function voltage in the first quadrant. I_S is the reverse bias saturation current. I_s and *n* were calculated from the intercept and the slope of the line shown

height. The diode turn-on voltage from Fig. 5 was seen to be 0.1 V.

Figure 6 shows the band diagram for PEDOT-PSS and MoS_2 before and after physical contact. Studies have shown the bandgap in PEDOT-PSS ~ 1.6 eV [25]. The absence of a field effect as seen in Fig. 3 implies that the Fermi level stays fixed midway between the HOMO and LUMO levels. MoS_2 was also seen to be an *n*-type material as verified in Fig. 4 with a bandgap of ~ 1.8 eV. The Fermi energy in MoS_2 is located closer to the conduction band edge in this semiconductor. The band diagram of PEDOT-PSS and MoS_2 together with key energy values for the components prior to the formation of the hetero-junction is shown in Fig. 6a. Upon physical contact, in thermal equilibrium, the Fermi energies of PEDOT-PSS and MoS_2 must coincide at the hetero-junction. When this happens, electrons from MoS_2 flow into the LUMO level of the polymer lowering its Fermi energy via band bending. A barrier is then formed that prevents further flow of electrons as seen in Fig. 6b. From the key energy values shown in Fig. 6a, the expected barrier height is 0.4 eV. The MoS_2 surface states and the PEDOT-PSS work function are some of the parameters that determine this barrier height [18, 26]. These remain unaffected by moisture even though the measurements were made in air.

Using the standard thermionic emission model of a Schottky junction, we have analyzed the diode performance. According to this model [27]:

$$J = J_s\left[\exp\frac{qV}{nkT} - 1\right] \tag{1}$$

$$J_s = A^*T^2\exp\left[\frac{-q\varphi}{kT}\right] \tag{2}$$

where J_s is the saturation current density, J is the current density, q is the electronic charge, k is the Boltzmann constant, T is the temperature (300 K), φ is the barrier height and n is the ideality parameter that takes into account corrections to the original simple model, e.g., lowering of the image-force barrier. The Richardson constant $A* \left(=\frac{4\pi qm^*k^2}{h^3}\right)$ is 120 A/K^2 cm^2 where m^* is the electron mass. At low voltage, a linear current increase in the diode is predicted by Eq. 1. Once the Schottky barrier is overcome, the current should increase exponentially. However, this increase is gradual (above 0.1 V) due to heating losses in the semiconductor. Figure 5 (inset) also shows the semi-logarithmic plot of the diode current versus applied voltage in the first quadrant. For low voltages ($V < 0.1$ V) and extrapolating the linear section to 0 V, we extract a saturation current (I_S) of 0.18 pA. The diode ideality parameter was calculated as follows:

$$n = \frac{q}{kT}\left[\frac{\partial V}{\partial \ln J}\right] \tag{3}$$

and was 1.9. Using these equations, the barrier height was 0.18 eV. It is known that some polymers tend to lower the work function of PEDOT-PSS [28]. The lower-than-expected value for the barrier height could be due to the presence of PEO that lowers the PEDOT-PSS work function below 5.1 eV that we assumed. Values of $n > 1$ have been attributed to several factors that include the recombination of holes and electrons in the depletion layer [29], the presence of an interfacial layer and interface states at the polymer–semiconductor interface [30] or even a tunneling process [31]. PEDOT-PSS nano-ribbons can detect alcohol vapors [32], and therefore, it makes this diode attractive for

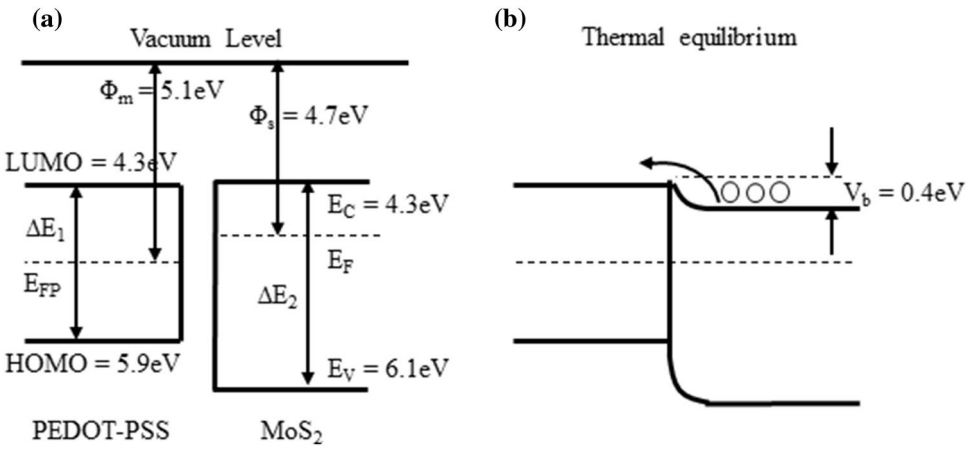

Fig. 6 The hetero-junction band diagram when MoS_2 is crossed with PEDOT-PSS: **a** before crossing **b** after crossing. E_F, E_C and E_V are the Fermi, conduction and valence energy levels of MoS_2 and E_{FP} is the Fermi energy of PEDOT-PSS. ΔE_1 (1.6 eV) and ΔE_2 (1.8 eV) are the energy bandgaps for PEDOT-PSS and MoS_2, respectively, φm (5.1 eV) and φs (4.7 eV) are the work functions of PEDOT-PSS and MoS_2, and V_b (0.4 eV) is the expected built-in potential barrier. A common Fermi level exists at thermal equilibrium via band bending. This gives rise to a Schottky barrier (indicated by the arrow) that blocks the flow of electrons from MoS_2 into the polymer

use as a gas sensor, thereby rendering it multifunctional. Using Ag contact electrodes (instead of Au) imply efficient charge injection into MoS_2 due to its lower Fermi energy and low contact resistance. Also, MoS_2 has a lower band-gap compared to WS_2; hence, the barrier height for electrons to flow into the LUMO level of PEDOT-PSS is lowered. This manifests itself as a smaller turn-on voltage as seen in Fig. 5 and better performance compared to the WS_2/PEDOT-PSS diode.

4 Conclusions

PEDOT-PSS was conducting with no field-dependent charge transport. MoS_2, however, was shown to be *n*-type and had a charge mobility of 0.5 cm^2/V s. Forming a junction of these two materials lead to a Schottky junction having an on/off ratio of 20 and a turn-on voltage of 0.1 V. Using the thermionic emission Schottky junction model, we calculated that the diode had $n = 1.9$ and a barrier height of 0.18 eV. A low turn-on voltage and small barrier height make this diode superior to that fabricated from WS_2/PEDOT-PSS. The PEDOT-PSS nano-ribbon and MoS_2 have large surface areas; this also makes the diode potentially useful as a gas sensor. The diode could be multifunctional in nature making it suitable for use in complex electronic circuits. Efforts are underway to fabricate an array of such diodes for signal processing.

Acknowledgements This work was funded in part by the National Science Foundation (NSF) under grants DMR-PREM 1523463 and DMR-RUI 1800262. A.T.C.J. and M.-Q.Z. acknowledge support from the NSF EFRI 2-DARE 1542879.

Compliance with ethical standards

Conflict of interest The authors declare that they have no conflict of interest.

References

1. Mak KF, Lee C, Hone J, Shan J, Heinz TF (2010) Atomically thin MoS_2: a new direct-gap semiconductor. Phys Rev Lett 105:136805
2. Ganatra R, Zhang Q (2014) Few-layer MoS_2: a promising layered semiconductor. ACS Nano 8:4074–4099
3. Radisavljevic B, Radenovic A, Brivio J, Giacometti V, Kis A (2011) Single-layer MoS_2 transistors. Nat Nanotechnol 6:147–150
4. Frindt RF (1966) Single crystals of MoS_2 several molecular layers thick. J Appl Phys 37:1928–1929
5. Novoselov KS, Jiang D, Schedin F, Booth TJ, Khotkevich VV, Morozov SV, Geim AK (2005) Two-dimensional atomic crystals. Proc Natl Acad Sci USA 102:10451–10453
6. Ayari A, Cobas E, Ogundadegbe O, Fuhrer MS (2007) Realization and electrical characterization of ultrathin crystals of layered transition-metal dichalcogenides. J Appl Phys 101:014507
7. Coleman JN, Lotya M, O'Neill A, Bergin SD, King PJ, Khan U, Young K, Gaucher A, De S, Smith RJ et al (2011) Two-dimensional nanosheets produced by liquid exfoliation of layered materials. Science 331:568
8. Zhan Y, Liu Z, Najmaei S, Ajayan PM, Lou J (2012) Large-area vapor-phase growth and characterization of MoS_2 atomic layers on a SiO_2 substrate. Small 8:966–971
9. Liu K-K, Zhang W, Lee Y-H, Lin Y-C, Chang M-T, Su C-Y, Chang C-S, Li H, Shi Y, Zhang H, Lai C-S, Li L-J (2012) Growth of large-area and highly crystalline MoS_2 thin layers on insulating substrates. Nano Lett 12:1538–1544
10. Lee Y-H, Zhang X-Q, Zhang W, Chang M-T, Lin C-T, Chang K-D, Yu Y-C, Wang JT-W, Chang C-S, Li L-J, Lin T-W (2012) Synthesis of large-area MoS_2 atomic layers with chemical vapor deposition. Adv Mater 24:2320–2325
11. Najmaei S, Liu Z, Zhou W, Zou X, Shi G, Lei S, Yakobson BI, Idrobo J-C, Ajayan PM, Lou J (2013) Vapour phase growth and grain boundary structure of molybdenum disulphide atomic layers. Nat Mater 12:754–759
12. Ling X, Lee Y-H, Lin Y, Fang W, Yu L, Dresselhaus MS, Kong J (2014) Role of the seeding promoter in MoS_2 growth by chemical vapor deposition. Nano Lett 14:464–472
13. Kam KK, Parkinson BA (1982) Detailed photocurrent spectroscopy of the semiconducting group VIB transition metal dichalcogenides. J Phys Chem 86:463–467
14. Pinto NJ, González R, Johnson AT Jr, MacDiarmid AG (2006) Electrospun hybrid organic/inorganic semiconductor Schottky nanodiode. Appl Phys Lett 89:033505
15. Neamen DA (2003) Semiconductor physics and devices, 3rd edn. McGraw Hill, New York
16. Ortiz DN, Vedrine J, Pinto NJ, Naylor CH, Johnson ATC (2016) Monolayer WS_2 crossed with an electro-spun PEDOT-PSS nano-ribbon: fabricating a Schottky diode. Mater Sci Eng B 214:68–73
17. Haynes WM (2014) CRC handbook of chemistry and physics. CRC Press, Boca Raton
18. Sze SM (1981) Physics of semiconductor devices. Wiley, New York
19. Han GH, Kybert NJ, Naylor CH, Lee BS, Ping J, Park JH, Kang J, Lee SY, Lee YH, Agarwal R, Charlie Johnson AT (2015) Seeded growth of highly crystalline molybdenum disulphide monolayers at controlled locations. Nat Commun 6:6128
20. Serrano W, Pinto NJ, Naylor CH, Kybert NJ, Johnson ATC Jr (2015) Facile fabrication of a ultraviolet tunable MoS_2/p-Si junction diode. Appl Phys Lett 106:193504
21. Lee C, Yan H, Brus LE, Heinz TF, Hone J, Ryu S (2010) Anomalous lattice vibrations of single- and few-layer MoS_2. ACS Nano 4:2695–2700
22. Lee YT, Hwang DK, Im S (2015) High-performance a MoS_2 nanosheet-based nonvolatile memory transistor with a ferroelectric polymer and graphene source–drain electrode. J Korean Phys Soc 67:L1499–L1503
23. Vega O, Wong F, Vega E, Luciano J, Rodriguez S, Pinto NJ, Rosa LG (2017) Electronic transport and anisotropic conductivity behavior on PEDOT:PSS nanoribbons and nanostructuring modification by atomic force microscope nanoshaving. Polym Sci ISSN 2471–9935(3):1–8
24. Joo J, Epstein AJ (1994) Electromagnetic radiation shielding by intrinsically conducting polymers. Appl Phys Lett 65:2278–2280
25. Groenendaal L, Jonas F, Freitag D, Pielartzik H, Reynolds JR (2000) Poly(3,4-ethylenedioxythiophene) and its derivatives: past, present, and future. Adv Mater 12:481–494
26. Saglam M, Biber M, Cakar M, Turut A (2004) The effects of the ageing on the characteristic parameters of polyaniline/p-type Si/Al structure. Appl Surf Sci 230:404–410
27. Scheinert S, Paasch GP (2004) Fabrication and analysis of polymer field-effect transistors. Phys State Solid (A) 201:1263–1301

28. Li Z, Liang Y, Zhong Z, Qian J, Liang G, Zhao K, Shi H, Zhong S, Yin Y, Tian W (2015) A low-work-function, high-conductivity PEDOT:PSS electrode for organic solar cells with a simple structure. Synth. Metals 210:363–366
29. Horowitz G (1990) Organic semiconductors for new electronic devices. Adv Mater 2:287–292
30. Gupta RK, Singh RA (2004) Junction properties of Schottky diode based on composite organic semiconductors: polyaniline-polystyrene system. J Polym Res 11:269–273
31. Halliday DP, Gray JW, Adams P, Monkman AP (1999) Electrical and optical properties of a polymer semiconductor interface. Synth Met 102:877–878
32. Pinto NJ, Rivera D, Melendez A, Ramos I, Lim JH, Charlie Johnson AT (2011) Electrical response of electrospun PEDOT-PSSA nanofibers to organic and inorganic gases. Sens Actuators, B 156:849–853